CORA Cork Open Research Archive
Cartlann Taighde Oscailte Chorcaí

Title	Ionic liquid based polymer gel electrolytes for use with germanium thin film anodes in lithium ion batteries
Authors	McGrath, Louise M.;Jones, John;Carey, Edwin;Rohan, James F.
Publication date	2019-12-13
Original Citation	McGrath, L. M., Jones, J., Carey, E. and Rohan, J. F. (2019) 'Ionic Liquid Based Polymer Gel Electrolytes for Use with Germanium Thin Film Anodes in Lithium Ion Batteries', ChemistryOpen, 8(12), pp. 1429-1436. doi: 10.1002/open.201900313
Type of publication	Article (peer-reviewed)
Link to publisher's version	https://chemistry-europe.onlinelibrary.wiley.com/doi/abs/10.1002/open.201900313 - 10.1002/open.201900313
Rights	© 2019 The Authors. Published by Wiley-VCH Verlag GmbH & Co. KGaA. This is an open access article under the terms of the Creative Commons Attribution#NonCommercial#NoDerivs License, which permits use and distribution in any medium, provided the original work is properly cited, the use is non# commercial and no modifications or adaptations are made - https://creativecommons.org/licenses/by-nc-nd/4.0/
Download date	2026-10-31 04:01:49
Item downloaded from	https://hdl.handle.net/10468/10965

UCC
University College Cork, Ireland
Coláiste na hOllscoile Corcaigh

ChemPubSoc Europe

DOI: 10.1002/open.201900313

Open Access ChemistryOPEN Full Paper

Ionic Liquid Based Polymer Gel Electrolytes for Use with Germanium Thin Film Anodes in Lithium Ion Batteries

Louise M. McGrath,[a] John Jones,[b] Edwin Carey,[b] and James F. Rohan*[a]

Thermally stable, flexible polymer gel electrolytes with high ionic conductivity are prepared by mixing the ionic liquid 1-butyl-1-methylpyrrolidinium bis(trifluoromethylsulfonyl)imide (C_4mpyrTFSI), LiTFSI and poly(vinylidene difluoride-co-hexafluoropropylene (PVDF-HFP). FT-IR and Raman spectroscopy show that an amorphous film is obtained for high (60%) C_4mpyrTFSI contents. Thermogravimetric analysis (TGA) confirms that the polymer gels are stable below ~300 °C in both nitrogen and air environments. Ionic conductivity of 1.9×10^{-3} S cm^{-2} at room temperature is achieved for the 60% ionic liquid loaded gel. Germanium (Ge) anodes maintain a coulombic efficiency above 95% after 90 cycles in potential cycling tests with the 60% C_4mpyrTFSI polymer gel.

1. Introduction

Due to the emergence of the Internet of Things (IoT) with in excess of 30 billion connected devices expected by 2020,[1] there is an increased focus on miniaturised wireless sensors. Coupling energy harvesters with microbatteries is an option to power the miniaturised sensors. Efficient power management systems will also be required to enable long-life IoT sensors. Metallic Li offers one of the largest gravimetric capacities for anode materials[2] and has been utilised in commercial microbatteries. However, for microbatteries, volume or area is more important than weight.[3] Li metal with a theoretical volumetric capacity of 2,062 mA h cm^{-3} is surpassed by Ge for which the capacity is 8,650 mA h cm^{-3}.[4] For microfabrication highly pure Ge can be readily sputter deposited in thin film format. As an anode material Ge exhibits favourable properties such as high conductivity based on the charge carrier mobility[5] and lithium storage gravimetric capacity of 1,620 mAh g^{-1} ($Li_{22}Ge_5$).[6] Ge thin films have been used to demonstrate high rate capability,[7] due to high lithium diffusivity,[7a] and thin native oxide layer which leads to a lower irreversible capacity during the first cycle.[8]

Despite these advantages, utilisation of Ge as an anode material has been hindered by the fact that it undergoes expansion and contraction upon Li alloying and de-alloying.[9] This leads to cracking and pulverisation of the electrode material which adversely influences the performance and cycle life. Alleviation or buffering of these effects may facilitate the use of Ge as anode material. Le Thai et al.[10] utilised polymer gel electrolytes to improve the cycle performance of MnO_2 based nanowire capacitors. By replacing a liquid electrolyte with a PMMA based gel electrolyte the capacitor cycle life was extended from 8,000 to more than 100,000 cycles with a coulombic efficiency of ~96%. The polymer gel buffered the expansion effects experienced by the material and maintained the electrode integrity.

Polymer gel electrolytes offer varying degrees of flexibility and higher ionic conductivities than solid state electrolytes.[11] Other essential criteria include good thermal, interfacial and electrochemical stabilities. In this work the PVDF-HFP, C_4mpyrTFSI ionic liquid and LiTFSI salt combination is used to form polymer gels. PVDF-HFP offers a high dielectric constant, for effective dissociation of Li salts generating a large quantity of carriers for conduction via the strong electron withdrawing groups.[12] It has been widely utilised as a polymer matrix[13] with Li salts and either standard organic-based electrolytes or room temperature ionic liquids (RTIL).

In general, RTILs offer favourable properties such as low-volatility, non-flammability, large electrochemical window and high ionic conductivity depending on the cation/anion combination. In the case of C_4mpyrTFSI a large electrochemical stability window[14] and operation over a wide temperature range[15] has been demonstrated.

A MacFarlane et al.[15] review discusses the cation/anion combinations that are best suited for use within Li and Li-ion batteries, as well as alternative battery chemistries. A further review by MacFarlane et al.[16] discusses ionic liquids which offer similar properties when their polymer gel analogues are created. Specifically, Pont et al.[17] investigated the properties of pyrrolidinium-based polymeric ionic liquids as polymer electrolytes. Their work highlighted that mechanically stable polymer gels with high ionic conductivities (10^{-4} S cm^{-1}) and large electrochemical windows (~7 V) can be obtained, which is favourable for solid state lithium batteries. Ferrari et al.[18]

[a] L. M. McGrath, Dr. J. F. Rohan
Electrochemical Materials and Energy Group
Tyndall National Institute
University College Cork, Lee Maltings, T12 R5CP, Cork, Ireland
E-mail: james.rohan@tyndall.ie
[b] J. Jones, Dr. E. Carey
Process Analytical Technology Lab
TU Dublin – Tallaght Campus
Blessington Rd, Tallaght, D24 FKT9, Dublin, Ireland

Supporting information for this article is available on the WWW under https://doi.org/10.1002/open.201900313

© 2019 The Authors. Published by Wiley-VCH Verlag GmbH & Co. KGaA. This is an open access article under the terms of the Creative Commons Attribution Non-Commercial NoDerivs License, which permits use and distribution in any medium, provided the original work is properly cited, the use is non-commercial and no modifications or adaptations are made.

demonstrated improved cycling behaviour of $LiFePO_4$ electrodes over 180 cycles with ionic liquid based polymer gel electrolytes when compared to their liquid counterparts. Sirisopanaporn et al.[19] demonstrated the safety of ionic liquid based polymer gels, as it was observed that a protective solid-electrolyte interface (SEI) layer forms on the surface of lithium metal anodes, in addition to no electrolyte leakage being observed after 4 months of storage. For further studies regarding the development of ionic liquid based polymer gel electrolytes, Ye et al.[20] and Marr et al.[21] provide a comprehensive discussion and reference list which highlight the benefits of these polymer gel electrolytes for battery applications.

A combination of PVDF-HFP with C_4mpyrTFSI has been investigated by Kim et al.[22] using a two-step process where a fibrous PVDF-HFP membrane was synthesised via electrospinning methods. The formed membranes were then soaked in 1 M LiTFSI/C_4mpyrTFSI to create an ionic liquid-based polymer gel electrolyte. The polymer gel composition and the resultant properties such as ionic conductivity, thermal and electrochemical stability can be more easily tailored using the single step solvent casting method described in this work. The improved characteristics are attributed to changes in the crystalline structure of the polymer gel due to the quantity of C_4mpyrTFSI utilised.

This work describes a simplified synthesis of the polymer gels which demonstrate favourable properties for lithium ion batteries. Most methods in the literature rely on high temperatures during synthesis,[11a] or drying the polymer gels under vacuum or high temperatures.[11b,13a,23] Our method can be performed outside of a glovebox at moderate temperatures (50 °C), with no vacuum or external heating required during the drying process, and no further treatment (e.g. soaking in electrolyte, or UV irradiation) once dry.

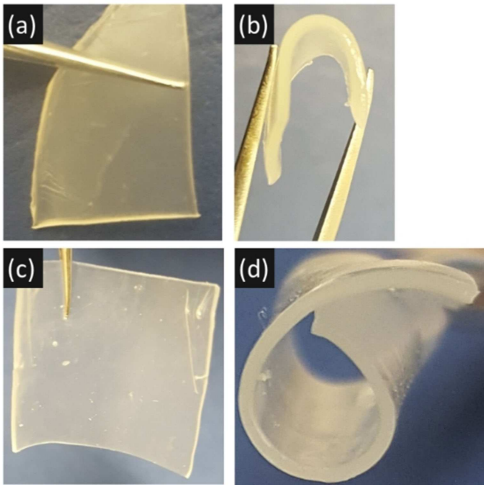


Figure 1. Optical images of synthesised 400 μm thick polymer gel electrolytes (a and b) PG-10, and (c and d) PG-60. Films of various thicknesses were synthesised and 42 μm films were used and discussed below for Figure 5.

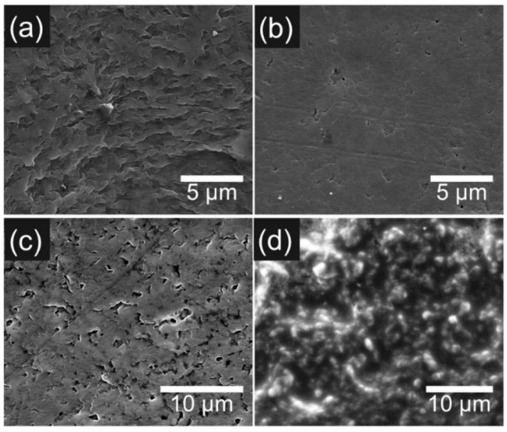


Figure 2. SEM micrographs of (a) PVDF-HFP, (b) PVDF-HFP with LiTFSI, (c) PG-10, (d) PG-60 films.

2. Results and Discussion

A series of polymer gels were synthesized, where the C_4mpyrTFSI content was varied between 10% and 60%. They were labelled as PG-X where X denoted the C_4mpyrTFSI content. For example, gels with 10% and 60% C_4mpyrTFSI are called PG-10 and PG-60, respectively. Gels which contained more than 60% C_4mpyrTFSI resulted in pastes rather than films. For comparison films consisting of PVDF-HFP, and PVDF-HFP with LiTFSI were also synthesised. Figure 1 displays the flexible polymer gels with the lowest and highest C_4mpyrTFSI content, PG-10 and PG-60.

SEM was utilised to assess the effects of LiTFSI salt and C_4mpyrTFSI on the morphology of the films. PVDF-HFP, PVDF-HFP with LiTFSI, PG-10 and PG-60 films were investigated and the resulting SEM images are shown in Figure 2. The pure PVDF-HFP film exhibits a flake-like surface (Figure 2a); however, upon addition of LiTFSI there is a distinct change to a more smooth surface morphology of the film (Figure 2b). When 10% C_4mpyrTFSI is introduced to the polymer gel the porosity of the polymer gel increases (Figure 2c). Despite the increased porosity the morphology of the films in 2(b) and (c) remain similar. The surface morphology for PG-60 (Figure 2d) is significantly more rough which suggests that addition of LiTFSI and C_4mpyrTFSI can lead to differences in the polymer's structure.

The crystallinity change of the polymer gel membranes upon addition of LiTFSI and C_4mpyrTFSI was analysed using IR and Raman spectroscopy. PVDF-HFP can exhibit different crystalline phases[24] (α, β, γ, δ) where the non-polar α-phase is the common crystalline state observed under normal conditions. The structures of the α-, β- and γ-phase are shown in Figure A1. Different crystalline phases can be obtained if the polymer undergoes stress, such as stretching or straining. Each crystalline state yields distinctive peaks when analysed using IR.

The IR spectrum obtained for pure PVDF-HFP is shown in Figures 3(a) and (b). There are several notable peaks obtained including at: 762 cm^{-1} ($C\text{-}F_2$ bending mode, α-phase)[25], 796 cm^{-1} ($C\text{-}F_3$ stretching mode, α-phase),[25a,c,e,f] 855 cm^{-1} (α-phase),[25a], 872 cm^{-1} ($C\text{-}H_2$ wagging of vinylidene, amorphous HFP),[25b,g], 974 cm^{-1} (out of plane C–H bending or twisting, α-phase),[25a–c,f] 1058 cm^{-1} (symmetric stretching of $C\text{-}F_3$, amor-

© 2019 The Authors. Published by Wiley-VCH Verlag GmbH & Co. KGaA

phous HFP),[25b] 1178 cm^{-1} (asymmetric C–F stretching),[25b,26] 1383 cm^{-1} (C-H_2 wagging vibration),[25b,c,26] and 1404 cm^{-1} (C-H_2 scissoring vibration).[25b,c,26] Only α-phase peaks are observed in the pure PVDF-HFP film, however upon addition of the LiTFSI salt there are notable changes in the IR spectrum. In the first instance, there is an additional peak observed at 658 cm^{-1} which can be attributed to the β-phase of PVDF-HFP.[26] A weak peak at 811 cm^{-1} is also observed which can be attributed to the γ-phase. The appearance of these two peaks signifies that the addition of LiTFSI salt stresses the polymer matrix and changes the crystalline phase formed. A broad peak within the region of 3700 cm^{-1} to 3050 cm^{-1} (peak b) can be attributed to the $TFSI^-$ anion. A peak at 1640 cm^{-1} (peak c) is ascribed to the complexation of the LiTFSI salt with the polymer backbone.[11c] The intensity of this peak decreases with increasing C_4mpyrTFSI content as the combination of LiTFSI and C_4mpyrTFSI reduces the tendency to form complexes.[22] This phenomenon could explain why different surface morphologies were obtained, as the LiTFSI is complexed with the polymer backbone and subsequently non-complexed when the C_4mpyrTFSI content is increased. For both PG-10 and PG-60 the FT-IR spectra are similar to the spectra for PVDF-HFP with LiTFSI, whereby peaks for amorphous (peak a), β- and γ-phases are observed. This trend is observed across the polymer gel series (Figure A2). For PG-60, the β- and γ-phase peaks are less intense than those for PG-10, however, the peaks denoting amorphicity yield higher intensities, which suggest that it adopts a more amorphous structure than PG-10.

Figure 3c shows the Raman data obtained for the films, where the same films were analysed in order to obtain further structural information. For the PVDF-HFP film, the strong peak obtained at 793 cm^{-1} can be attributed to C-H_2 rocking and C-F_2 stretching modes, which is indicative of α-phase PVDF-HFP. Similarly, peaks at 873 cm^{-1} and 1426 cm^{-1} are due to a combination of C–C symmetric stretching and C–C–C skeletal bonding modes, C-H_2 scissoring and C-H_2 wagging modes respectively[27] which indicate that our pure PVDF-HFP films exists in the α-phase. Upon addition of LiTFSI some of the previously observed peaks are dampened, whereby the peak at 793 cm^{-1} is no longer observed but rather a doublet peak at 811 cm^{-1} and 836 cm^{-1}. This is observed as the crystalline state of the PVDF-HFP film changes from α-phase to a mixture of β- (836 cm^{-1})[27a] and γ-phase (811 cm^{-1}).[27b] Furthermore, the peak observed at 873 cm^{-1} in the PVDF-HFP data, shifts to 878 cm^{-1} which is indicative of a shift from α-phase to γ-phase.[27b] This follows a similar trend noted in the IR data where peaks for both crystalline states were observed, while peaks pertaining to α-phase were dampened or not observed. A weak peak at 743 cm^{-1} (peak b) is attributed to the $TFSI^-$ anion[22,27b,28] and this peak yields information regarding the conformational state of the anion. A peak observed at 747 cm^{-1} would suggest that the anion is co-ordinated to Li cation,[22] which would reduce ionic conductivity and mobility. Peaks obtained at 739 cm^{-1} and

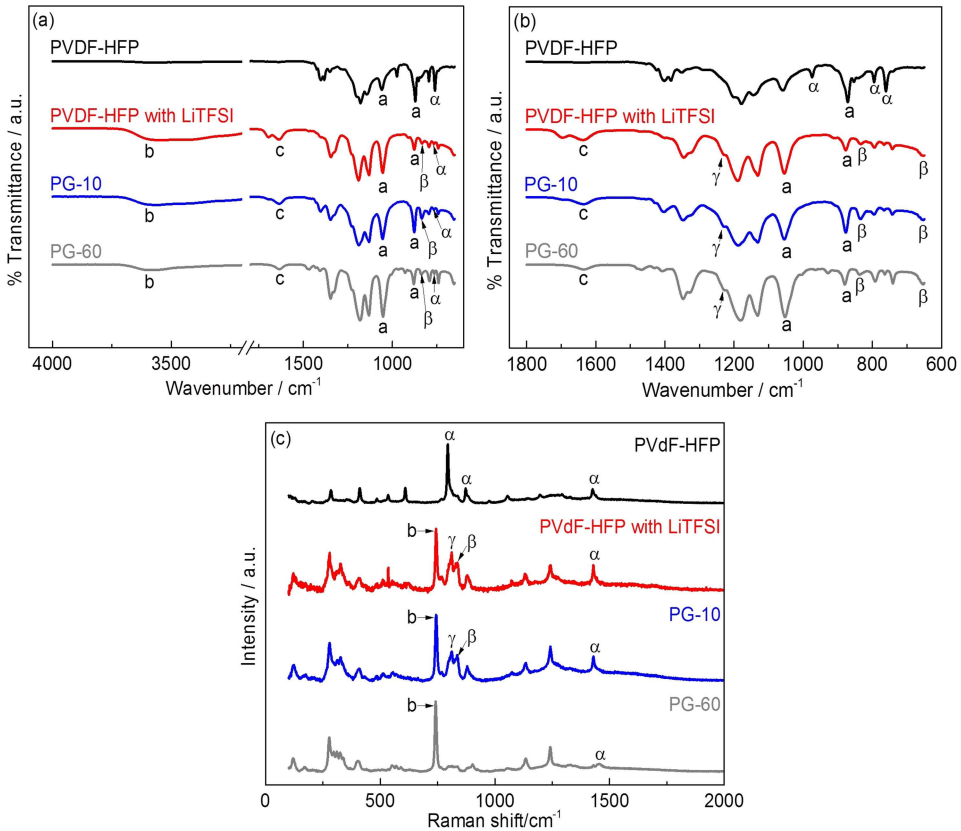


Figure 3. Room temperature FT-IR spectra of PVDF-HFP, PVDF-HFP with LiTFSI, PG-10 and PG-60, (a) displaying the range 4000 cm^{-1} to 650 cm^{-1}, (b) displaying the range 1800 cm^{-1} to 650 cm^{-1}, (c) room temperature Raman spectra of PVDF-HFP, PVDF-HFP with LiTFSI, PG-10 and PG-60.

© 2019 The Authors. Published by Wiley-VCH Verlag GmbH & Co. KGaA

743 cm^{-1} suggest that the anion is not co-ordinated to the Li cation, and adopts a cisoid and transoid conformational state.[29] A peak at 743 cm^{-1} is observed which suggests that the $TFSI^-$ anion adopts a transoid conformation where the CF_3 groups are on opposite sides of the S–N–S plane. When 10% C_4mpyrTFSI is added to the gel, the intensity of this peak increases due to the higher concentrations of $TFSI^-$ anions present. This trend is observed across a series of polymer gels where the C_4mpyrTFSI content was increased. The PG-10 film data is similar to that obtained for PVDF-HFP with LiTFSI, however the intensities of the peaks increases as seen for the peaks between 250 cm^{-1} and 440 cm^{-1} which are attributed to C–C aliphatic chains. The pyrrolidinium ring is considered to be aliphatic as it does not contain C=C bonds, hence increasing the content of C_4mpyrTFSI leads to increased intensities observed in Raman spectra (Figure A3). The peaks corresponding to both β- (836 cm^{-1}) and γ-phase (811 cm^{-1}) are observed for PG-10 which suggests that its structure is similar to PVDF-HFP with LiTFSI. The Raman data obtained for PG-60 show these peaks with similar intensities as PVDF-HFP with LiTFSI, though the gels have different crystal structures. There are no prominent α-phase peaks observed but rather a weak peak at 1429 cm^{-1}. This suggests that PG-60 adopts a predominantly amorphous structure with some crystallinity due to the presence of PVDF.

The DSC plots obtained for pure PVDF-HFP, PVDF-HFP with LiTFSI, PG-10, and PG-60 are shown in Figure 4a. From this data, the large exothermic peak obtained is attributed to the melting point of the polymers. Pure PVDF-HFP yields a melting point of 149 °C, which decreases slightly to 147 °C upon addition of LiTFSI salt. Similar trends are observed when C_4mpyrTFSI is added to the polymer gel, as the melting points for PG-10 and PG-60 are 146 °C and 120 °C, respectively. The decrease in the melting temperature is attributed to phase changes within the polymer gel. As the amorphicity is increased the melting temperature decreases as observed by Kim et al.[22] Similarly, the degree of crystallinity was determined from the DSC data, using Equation 1:

$$Xc(\%) = \frac{\Delta H_m}{\Delta H_{m.ref}} \times 100 \quad (1)$$

Upon addition of LiTFSI salt and C_4mpyrTFSI the degree of crystallinity decreased from 34% for PG-10 to 11% for PG-60. This demonstrates that PG-60 adopts an amorphous structure. This data is in good agreement with the FT-IR and Raman data, with the crystallinity of the films decreasing upon addition of the LiTFSI salt and C_4mpyrTFSI and for which the PG-60 film shows the highest degree of amorphicity.

The TGA plots of pure PVDF-HFP, PVDF-HFP with LiTFSI, PG-10, and PG-60 in N_2 are shown in Figure 4b. PVDF-HFP degrades in two steps, where the first step occurs between 100 °C to 300 °C and the other at ~450 °C. The weight loss observed between 100 and 300 °C is attributed to the loss of residual acetone from the film synthesis trapped within the PVDF-HFP

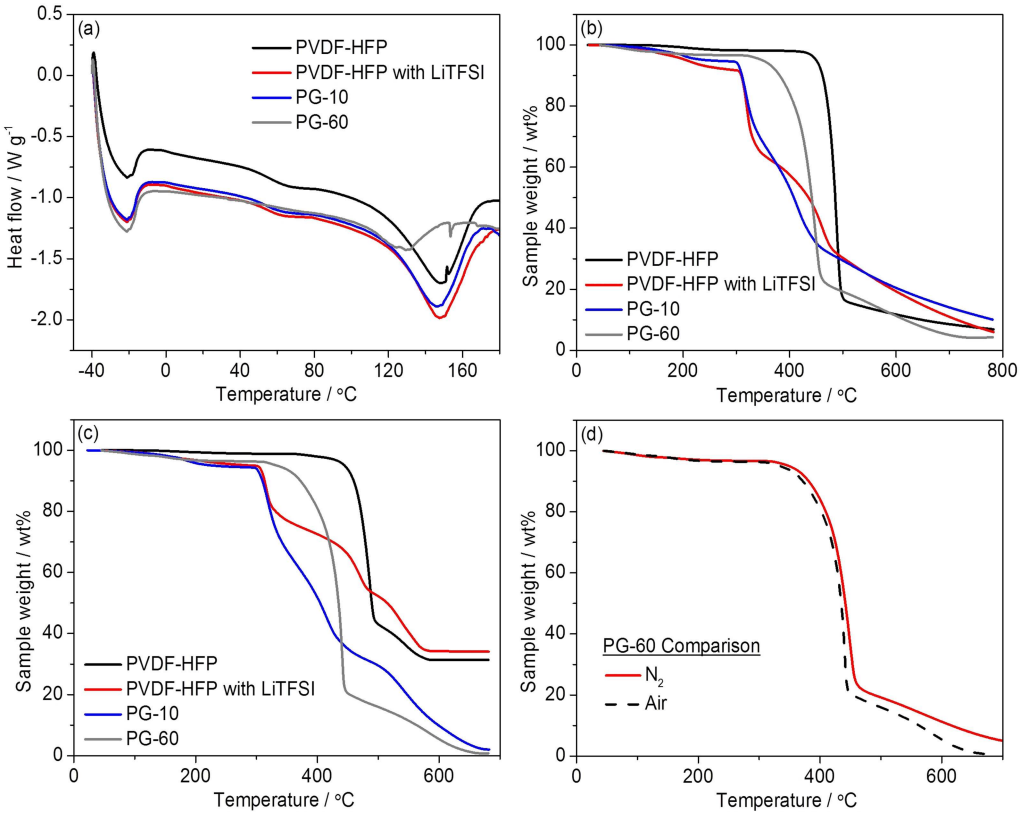


Figure 4. (a) DSC traces of pure PVDF-HFP, PVDF-HFP with LiTFSI, PG-10, and PG-60, (b–d) TGA plots obtained under (b) N_2 and (c) air, where the N_2 flow rate was 10 ml min^{-1}, (d) comparison of TGA plots for PG-60 obtained under N_2 and air.

© 2019 The Authors. Published by Wiley-VCH Verlag GmbH & Co. KGaA

matrix.[30,31] The degradation at ~450 °C is attributed to the decomposition of PVDF-HFP.[22] From the data it is clear that the PVDF-HFP has not degraded completely with more than 30% weight remaining. This results from the formation of a char, which is characteristic of linear aromatic and cyclic structures on degradation in nitrogen.[31] Upon addition of the LiTFSI salt, the thermal stability of the polymer gel decreases, whereby the onset of thermal degradation occurs at ~300 °C. This change in the thermal stability is attributed to the change in the crystallinity of the films described above. The addition of the LiTFSI salt to PVDF-HFP causes stress, which leads to the observation of other crystalline forms. This stress is caused by LiTFSI salt complexing with the PVDF-HFP backbone which has been observed previously by Shalu et al.[11c] Similarly when a small amount of C_4mpyrTFSI is added to the polymer gel, a low thermal stability is noted with decomposition at ~300 °C. This result is expected as PVDF-HFP with LiTFSI and PG-10 yield similar crystal structures. When a higher amount of C_4mpyrTFSI is present in the gel, the thermal stability of the polymer increases and is closer to that observed for pure PVDF-HFP films. This is attributed to the change in crystalline structure as the polymer gel exhibits a predominantly amorphous and α-phase structure similar to that of pure PVDF-HFP. The onset of thermal degradation at ~350 °C is due to the C_4mpyrTFSI, with subsequent degradation from PVDF-HFP.[22] Both the PG-10 and PG-60 exhibit a large operating temperature range which is advantageous for battery applications.

TGA analysis on the polymer gels was carried out in air determine if the packaging environment of the battery would affect the operational temperature of the polymer gel. Similar results are obtained where the degradation of the polymer gels follow the same mechanisms. Both polymer gels with C_4mpyrTFSI exhibit thermal stability up to ~300 °C in air (Figure 4c). This is further observed when the temperature ramp rates are varied as there is no significant change in the thermal degradation onset temperature (Figure A4). The onset of decomposition for the polymer gels in air varies by less than 4 °C by comparison with those assessed under N_2 (Figure 4d). However, unlike under N_2 where char formation was observed, full decomposition of PG-60 occurred under air. This suggests that at elevated temperatures, storing or operating the polymer gel under air would have a greater effect on its performance and stability. At temperatures less than 400 °C, the polymer gel reacts similarly in air and N_2 environments.

The crystallinity of the polymer gels leads to differences in their surface morphology and thermal stability. To determine the effects of crystallinity on the electrochemical properties, the ionic conductivity of the polymer gel films was determined using EIS at room temperature. It is known that the crystalline regions of polymers are responsible for the mechanical stability, while the amorphous regions are responsible for ionic conduction.[11c] The addition of LiTFSI salt and C_4mpyrTFSI to the PVDF-HFP matrix is responsible for viable ionic conductivities. Table 1 shows the ionic conductivities for a typical solid-state[32] and organic electrolyte[33] in addition to the experimental values obtained for the polymer gel. From this table it can be seen that all versions of the polymer gel offer significantly higher ionic conductivities than solid-state LiPON.[34] This trend is observed across the series of polymer gels (Table 1). The polymer gel containing 60% C_4mpyrTFSI is almost 600 times more conductive, while the polymer gel containing 10% C_4mpyrTFSI is 23 times greater than LiPON. Comparing their ionic conductivities to that of 1 M $LiPF_6$ in EC:DEC (1:1 v/v) it is evident that the polymer gels are comparable to standard organic solvents. The ionic conductivity of the liquid C_4mpyrTFSI with 0.5 M LiTFSI salt (~1.5 mS cm^{-1}), which has been utilised as an electrolyte for Li-ion applications,[35] is lower than that for polymer gel PG-60 of this research.

The electrochemical performance for the ionic liquid based polymer gel electrolyte when cycled with Ge thin film is shown in Figure 5. PG-60 was sandwiched between Ge and Li to form a half cell. Figure 5a shows the initial scans with Ge, where a scan rate of 0.025 mV s^{-1} was utilized. The CV shows the characteristic CV data for amorphous Ge, with a pronounced peak at 1 V. This peak has been attributed to the electrolyte reduction reactions and it does not appear in subsequent cycles. The peak current observed is larger than what has been previously observed and the reduction layer products formed allow for a stable system to be obtained after 3 cycles. This is demonstrated by the overlapping CVs which are observed at all scan rates, even in the latter half of the cycling as shown in Figure 5b. Furthermore, the coulombic efficiency is greater than 95% after 90 cycles which demonstrates the cyclability of PG-60 with Ge. In addition, the capacity retention was maintained at an average of 86% across the various scan rates. Similar results were obtained with a PG-60 thickness of 42 μm, whereby higher capacities were obtained due to the reduction in electrolyte volume (Figure 5d), thus improving the overall volumetric capacity of the cell. The average cycling efficiency over 50 cycles was 82%, which is lower than that for the 400 μm thick PG-60 (95% over 90 cycles), however, the thinner electrolyte coupled with the Ge electrode helped maintain capacity values close to the theoretical capacity of Ge at 0.05 mV s^{-1} and 0.1 mV s^{-1} as shown in Figure.5d. Cycling at 0.5 mV s^{-1} yields higher capacity values (~850 mAh g^{-1}) than for the 400 μm PG-60 (~500 mAh g^{-1}) which demonstrates that the thinner electrolyte allow for higher specific capacities to be obtained. Further work is required to improve capacity retention, as capacity retention of 78% was obtained for the final 0.1 mV s^{-1} when compared to the initial 0.1 mV s^{-1} capacities, however, these

Table 1. Comparison of ionic conductivities of solid state,[32] polymer gel and organic solvent electrolytes.[33]

	LiPON	PG-10	PG-20	PG-30	PG-40	PG-50	PG-60	1 M $LiPF_6$ in (1:1 v/v) EC:DEC
Conductivity (mS cm^{-1})	3×10^{-3}	7×10^{-2}	7×10^{-2}	0.2	0.4	0.8	1.9	7.9

© 2019 The Authors. Published by Wiley-VCH Verlag GmbH & Co. KGaA

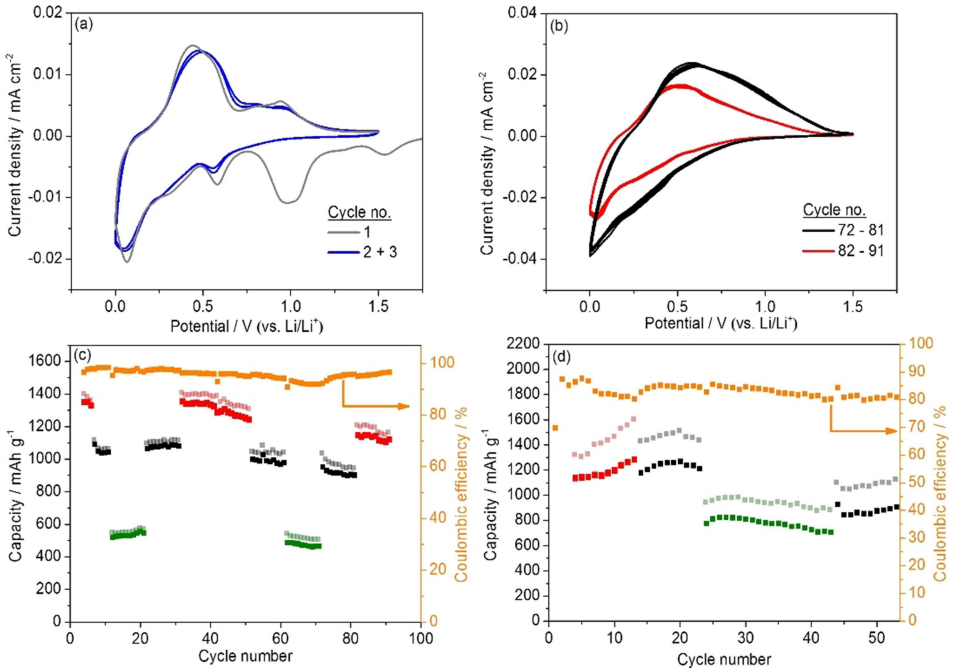


Figure 5. Electrochemical data obtained for 100 nm Ge with 400 µm thick PG-60, (a) initial 3 cycles obtained at 0.025 mV s^{-1} scan rate, (b) final cycles obtained at 0.05 mV s^{-1} (red) and 0.1 mV s^{-1} (black), (c) capacity values obtained for each scan rate: 0.05 mV s^{-1} (red), 0.1 mV s^{-1} (black), and 0.5 mV s^{-1} (green), the coulombic efficiency is indicated in on the right hand axis in orange, (d) capacity values obtained for each scan rate: 0.05 mV s^{-1} (red), 0.1 mV s^{-1} (black), and 0.5 mV s^{-1} (green), where PG-60 thickness was 42 µm, the coulombic efficiency is indicated in on the right hand axis in orange.

initial results demonstrate that thin films of PG-60 are viable for use as a solid state electrolyte. Both Figure 5c and 5d indicate that both the 400 µm and 42 µm PG-60 are capable of buffering the volumetric expansion effects experienced by Ge upon cycling with Li.

Galvanostatic cycling was carried out using PG-60 with a thickness of 320 µm as shown in Figure 6. Various C-rates were employed to determine the cyclability of the Ge with PG-60 at fast and slow rates. Figure 6a shows the initial cycles obtained for 0.15 C. The first 3 cycles indicate the formation of an SEI

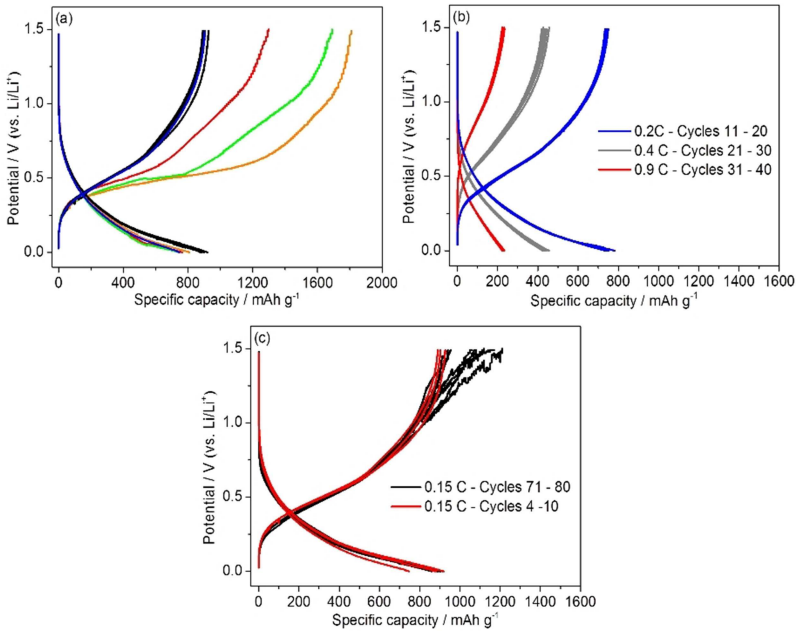


Figure 6. Galvanostatic cycling data obtained for 100 nm Ge with 320 µm thick PG-60, (a) initial charge/discharge cycles obtained at 0.15 C, where the red data corresponds to cycle 1, green to cycle 2, orange to cycle 3, black for cycles 4 to 9 and blue for cycle 10, (b) subsequent cycles obtained at 0.2 C (blue), 0.4 C (grey) and 0.9 C (red), (c) comparison of initial (red) and final (black) charge/discharge cycles obtained at 0.15 C.

© 2019 The Authors. Published by Wiley-VCH Verlag GmbH & Co. KGaA

layer as the initial charge capacity obtained is 1299 mAh g^{-1}, which increases to 1694 and 1809 mAh g^{-1}, for cycles 2 and 3. The coulombic efficiency for these cycles are 59%, 44% and 45% respectively. From cycle 4 onwards, the system stabilises and the charge/discharge profiles overlap as shown in Figure 6a. The charge and discharge capacities remain stable around 900 and 850 mAh g^{-1} respectively. The average coulombic efficiency for cycles 4 to 10 is 96%, which demonstrates the polymer gel compatibility with Ge. Similar stability is seen at increased C-rates as shown in Figure 6b. The 0.2 C data in Figure 6b, yields charge and discharge capacities of 756 and 750 mAh g^{-1} respectively, with a coulombic efficiency of 99.3%. This high coulombic efficiency is further evidence that the SEI layer formed in the initial cycles has led to a stable system. This is further evidenced in subsequent cycles at 0.4 C and 0.9 C data as high coulombic efficiencies are observed, 99.9% and 99.7% respectively. The specific capacities decrease to approximately 210 to 220 mAh g^{-1} for both charge and discharge cycles at the 0.9 C rate, and this corresponds to 13 to 14% of the theoretical capacity of Ge. This suggests that slower charge times may be suited for polymer gels of this thickness. Despite this, faster C-rates were investigated (1.8 C, 3.5 C and 5 C) followed immediately by scans at 0.15 C. The final 0.15 C cycling data is shown in Figure 6c. From this data, the system stability is demonstrated as there is good overlap between the initial and final 0.15 C data. Similarly, the charge and discharge capacities obtained are 1094 and 890 mAh g^{-1} respectively, with an average coulombic efficiency of 83%. The charge/discharge cycles demonstrate that PG-60 is capable of buffering the volumetric expansion effects experienced by Ge upon cycling with Li.

3. Conclusions

Flexible polymer gel electrolytes containing PVDF-HFP, C_4mpyrTFSI and LiTFSI salt were synthesised. The C_4mpyrTFSI content within the gel yields differences in the crystallinity, surface morphology, thermal stability and ionic conductivity. Despite this, both 10% and 60% C_4mpyrTFSI content polymer gels exhibited thermal stability up to 300 °C and ionic conductivities 23 and 600 times greater, respectively, than that of typical solid-state electrolytes. PG-60 exhibited electrochemical stability with a Ge electrode, whereby coulombic efficiencies greater than 95% were maintained over 90 cycles. Galvanostatic cycling further demonstrated that PG-60 is compatible with Ge, as coulombic efficiencies of >99% were obtained at various C-rates. Therefore this polymer gel electrolyte is capable of buffering the expansion effects experienced by Ge and is suitable for use as a flexible, high conductivity, thermally stable electrolyte for application in Li-ion microbatteries.

Experimental Section

Materials

1-butyl-1-methylpyrrolidinium bis(trifluoromethylsulfonyl)imide (C_4mpyrTFSI) was obtained from Solvionic (>99% purity). Li bis (trifluoromethylsulfonyl)imide (LiTFSI) and PVDF-HFP were obtained from Sigma Aldrich (>99% purity). All chemicals were stored under argon atmosphere and used as received.

Sample Preparation

The polymer gels were synthesised by dissolving PVDF-HFP in dried acetone at 50 °C with stirring for 30 minutes. Once dissolved, the LiTFSI was added and stirred for a further 30 minutes. Finally, C_4mpyrTFSI was added and the mixture was stirred for 1 hour. The solution was solvent cast into petri dishes and the acetone evaporated.

Material Characterisation

FT-IR data was recorded using a Perkin Elmer Spotlight for mid-IR wavelengths (4,000 to 400 cm^{-1}). Raman spectra of the polymer gels were recorded on a Horiba Raman Spectrometer with dual wavelengths (532 nm and 785 nm). Analysis was carried out using a 785 nm wavelength to avoid fluoresce emitted at lower wavelengths. Thermogravimetric Analysis (TGA) was carried out using a TA Instruments, model TA Q50 and platinum pans. The temperature ramp was varied (20, 40 and 60 °C min^{-1}) to obtain temperature profiles over the temperature range 30 °C to 800 °C. The polymer gels were analysed under N_2 and air. Differential Scanning Calorimetry (DSC) was carried out using a TA Instruments Q2000 with attached refrigerated cooling system. The samples were cooled to −40 °C and using temperature ramps of 20, 40 and 60 °C min^{-1}, the temperature was increased to 180 °C. The purge gas used was nitrogen with a flow rate of 10 ml min^{-1}.

Electrochemical Measurements

A Bio-Logic VSP multi-channel potentiostat was used for electrochemical impedance spectroscopy (EIS). The ionic conductivity of the polymer gels was determined over a frequency range of 150 kHz to 10 Hz, with an amplitude of 5 mV and using the following equation:

$$\sigma = \frac{A.R}{l} \tag{2}$$

Where A is the area of the polymer gel, R is the resistance measured and *l* is the thickness of the polymer gel sample. The thickness of the polymer gels were determined using a micrometer, and this value was used in Equation 2. The polymer gels were then sandwiched between two stainless steel electrodes and the measurements were carried out at open circuit potential. The ionic conductivity of a 0.5 M LiTFSI in C_4mpyrTFSI solution was also obtained to compare with the polymer gel ionic conductivities.

To determine the polymer gel viability as an electrolyte, it was analysed in a three electrode cell, where the working electrode consisted of DC sputtered Ge film and Li counter and reference electrodes (Sigma Aldrich, 99.9% trace metal basis). The cell assembly was carried out in a glovebox, where the oxygen and water levels were below 1 ppm. Cyclic voltammetry (CV) studies were also carried out using the Bio-Logic VSP multi-channel

© 2019 The Authors. Published by Wiley-VCH Verlag GmbH & Co. KGaA

potentiostat, where the potential was scanned between 0 V and 1.5 V vs. Li/Li^+ with scan rates of 0.05, 0.1 and 0.5 $mV s^{-1}$. Galvanostatic cycling tests were carried out using the Bio-Logic VSP multi-channel potentiostat, where various C-rates were utilised in the potential range: 1.5 V to 0 V.

Acknowledgements

This publication has emanated from research conducted with the financial support of Science Foundation Ireland (SFI) and is co-funded under the European Regional Development Fund under Grant Number 13/RC/2077.

Keywords: flexible polymers · gel electrolyte membranes · germanium anodes · ionic liquids · lithium-ion batteries

[1] Internet of Things (IoT) connected devices installed base worldwide from 2015 to 2025 (in billions), 2019, https://www.statista.com/statistics/471264/iot-number-of-connected-devices-worldwide/, 26/10/2018
[2] B. Laïk, I. Ressejac, C. Venet, J.-P. Pereira-Ramos, *Thin Solid Films* **2018**, *649*, 69–74.
[3] a) J. Zhu, J. Jiang, Y. Feng, G. Meng, H. Ding, X. Huang, *ACS Appl. Mater. Interfaces* **2013**, *5*, 2634–2640; b) W. Wang, M. Tian, A. Abdulagatov, S. M. George, Y.-C. Lee, R. Yang, *Nano Lett.* **2012**, *12*, 655–660; c) Y. Gogotsi, P. Simon, *Science* **2011**, *334*, 917–918.
[4] X. L. Wu, Y. G. Guo, L. J. Wan, *Chemistry – An Asian Journal* **2013**, *8*, 1948.
[5] a) I.-S. Hwang, J.-C. Kim, S.-D. Seo, S. Lee, J.-H. Lee, D.-W. Kim, *Chem. Commun.* **2012**, *48*, 7061–7063; b) Y.-D. Ko, J.-G. Kang, G.-H. Lee, J.-G. Park, K.-S. Park, Y.-H. Jin, D.-W. Kim, *Nanoscale* **2011**, *3*, 3371–3375; c) J. Wang, N. Du, H. Zhang, J. Yu, D. Yang, *J. Mater. Chem.* **2012**, *22*, 1511–1515.
[6] S. Yoon, C.-M. Park, H.-J. Sohn, *Electrochem. Solid-State Lett.* **2008**, *11*, A42–A45.
[7] a) J. Graetz, C. C. Ahn, R. Yazami, B. Fultz, *J. Electrochem. Soc.* **2004**, *151*, A698–A702; b) L. Baggetto, R. A. H. Niessen, F. Roozeboom, P. H. L. Notten, *Adv. Funct. Mater.* **2008**, *18*, 1057–1066.
[8] C.-M. Hwang, J.-W. Park, *Thin Solid Films* **2010**, *518*, 6590–6597.
[9] X. L. Sun, X. Y. Lu, S. Z. Huang, L. X. Xi, L. X. Liu, B. Liu, Q. H. Weng, L. Zhang, O. G. Schmidt, *ACS Appl. Mater. Interfaces* **2017**, *9*, 38556–38566.
[10] M. Le Thai, G. T. Chandran, R. K. Dutta, X. Li, R. M. Penner, *ACS Energy Lett.* **2016**, *1*, 57–63.
[11] a) Z. Ruisi, C. Yuanfen, R. Montazami, *Materials* **2015**, *8*, 2735–2748; b) P.-L. Kuo, C.-H. Tsao, C.-H. Hsu, S.-T. Chen, H.-M. Hsu, *J. Membr. Sci.* **2016**, *499*, 462–469; c) V. K. S. Shalu, R. K. Singh, *J. Mater. Chem. C* **2015**, *3*, 7305–7318.
[12] A. M. Stephan, K. Nahm, *Polymer* **2006**, *47*, 5952–5964.
[13] a) H. Ye, J. Huang, J. J. Xu, A. Khalfan, S. G. Greenbaum, *J. Electrochem. Soc.* **2007**, *154*, A1048–A1057; b) G. B. Appetecchi, G. T. Kim, M. Montanino, M. Carewska, R. Marcilla, D. Mecerreyes, I. De Meatza, *J. Power Sources* **2010**, *195*, 3668–3675; c) G. B. Appetecchi, G. T. Kim, M. Montanino, F. Alessandrini, S. Passerini, *J. Power Sources* **2011**, *196*, 6703–6709.
[14] M. Hayyan, F. S. Mjalli, M. A. Hashim, I. M. AlNashef, T. X. Mei, *Journal of Industrial and Engineering Chemistry* **2013**, *19*, 106–112.
[15] D. R. MacFarlane, N. Tachikawa, M. Forsyth, J. M. Pringle, P. C. Howlett, G. D. Elliott, J. H. Davis, M. Watanabe, P. Simon, C. A. Angell, *Energy Environ. Sci.* **2014**, *7*, 232–250.
[16] D. R. MacFarlane, M. Forsyth, P. C. Howlett, M. Kar, S. Passerini, J. M. Pringle, H. Ohno, M. Watanabe, F. Yan, W. Zheng, S. Zhang, J. Zhang, *Nat. Rev. Mater.* **2016**, *1*, 15005.
[17] A.-L. Pont, R. Marcilla, I. De Meatza, H. Grande, D. Mecerreyes, *J. Power Sources* **2009**, *188*, 558–563.
[18] S. Ferrari, E. Quartarone, P. Mustarelli, A. Magistris, M. Fagnoni, S. Protti, C. Gerbaldi, A. Spinella, *J. Power Sources* **2010**, *195*, 559–566.
[19] C. Sirisopanaporn, A. Fernicola, B. Scrosati, *J. Power Sources* **2009**, *186*, 490–495.
[20] Y.-S. Ye, J. Rick, B.-J. Hwang, *J. Mater. Chem. A* **2013**, *1*, 2719–2743.
[21] P. C. Marr, A. C. Marr, *Green Chem.* **2016**, *18*, 105–128.
[22] J.-K. Kim, L. Niedzicki, J. Scheers, C.-R. Shin, D.-H. Lim, W. Wieczorek, P. Johansson, J.-H. Ahn, A. Matic, P. Jacobsson, *J. Power Sources* **2013**, *224*, 93–98.
[23] M. Li, L. Yang, S. Fang, S. Dong, S.-i. Hirano, K. Tachibana, *Polym. Int.* **2012**, *61*, 259–264.
[24] J.-H. Cao, B.-K. Zhu, Y.-Y. Xu, *J. Membr. Sci.* **2006**, *281*, 446–453.
[25] a) P. Martins, A. C. Lopes, S. Lanceros-Mendez, *Prog. Polym. Sci.* **2014**, *39*, 683–706; b) S. Ramesh, O. P. Ling, *Polym. Chem.* **2010**, *1*, 702–707; c) M. A. Gebreyesus, Y. Purushotham, J. S. Kumar, *Heliyon* **2016**, *2*, e00134; d) S. Abbrent, J. Plestil, D. Hlavata, J. Lindgren, J. Tegenfeldt, Å. Wendsjö, *Polymer* **2001**, *42*, 1407–1416; e) L. Ruan, X. Yao, Y. Chang, L. Zhou, G. Qin, X. Zhang, *Polymer* **2018**, *10*, 228; f) D. Yuan, Z. Li, W. Thitsartarn, X. Fan, J. Sun, H. Li, C. He, *J. Mater. Chem. C* **2015**, *3*, 3708–3713; g) L. N. Sim, S. R. Majid, A. K. Arof, *Vib. Spectrosc.* **2012**, *58*, 57–66.
[26] A. Daneshkhah, S. Shrestha, A. Siegel, K. Varahramyan, M. Agarwal, *Sensors* **2017**, *17*, 595.
[27] a) J. Pitawala, M. A. Navarra, B. Scrosati, P. Jacobsson, A. Matic, *J. Power Sources* **2014**, *245*, 830–835; b) S. Das, A. Ghosh, T. J. M., A. M., *J. Appl. Phys.* **2016**, *119*, 095101.
[28] L. J. Hardwick, M. Holzapfel, A. Wokaun, P. Novák, *J. Raman Spectrosc.* **2007**, *38*, 110–112.
[29] M. Herstedt, M. Smirnov, P. Johansson, M. Chami, J. Grondin, L. Servant, J. C. Lassègues, *J. Raman Spectrosc.* **2005**, *36*, 762–770.
[30] W. Liu, X. K. Zhang, F. Wu, Y. Xiang, *IOP Conference Series: Materials Science and Engineering* **2017**, *213*, 012036.
[31] J. D. Menczel, R. B. Prime, *Thermal Analysis of Polymers: Fundamentals and Applications*, Wiley, **2014**.
[32] J. F. Oudenhoven, L. Baggetto, P. H. Notten, *Adv. Energy Mater.* **2011**, *1*, 10–33.
[33] K. Hayashi, Y. Nemoto, S.-I. Tobishima, J.-I. Yamaki, *Electrochim. Acta* **1999**, *44*, 2337–2344.
[34] J. F. Ribeiro, R. Sousa, J. P. Carmo, L. M. Gonçalves, M. F. Silva, M. M. Silva, J. H. Correia, *Thin Solid Films* **2012**, *522*, 85–89.
[35] A. Lahiri, N. Borisenko, A. Borodin, M. Olschewski, F. Endres, *Phys. Chem. Chem. Phys.* **2016**, *18*, 5630–5637.

Manuscript received: October 18, 2019
Revised manuscript received: November 19, 2019

© 2019 The Authors. Published by Wiley-VCH Verlag GmbH & Co. KGaA